Lin, Q., Musa, S. S., Zhao, S., & He, D. (2020). Modeling the 2014–2015 Ebola virus disease outbreaks in Sierra Leone, Guinea, and Liberia with effect of high-and low-risk susceptible individuals. Bulletin of Mathematical Biology, 82(8), 102.

Modeling the 2014-15 Ebola Virus Disease outbreaks in Sierra Leone, Guinea, and Liberia with effect of high- and low-risk susceptible individuals

Qianying Lin[1,2], Salihu S. Musa[2,3], Shi Zhao[2,4,5], & Daihai He[2,*]

1 Michigan Institute for Data Science, University of Michigan, Ann Arbor

2 Department of Applied Mathematics, The Hong Kong Polytechnic University, Hong Kong

3 Department of Mathematics, Kano University of Science and Technology, Wudil, Nigeria

4 JC School of Public Health and Primary Care, Chinese University of Hong Kong, Hong Kong, China

5 Shenzhen Research Institute of Chinese University of Hong Kong, Shenzhen, China

∗ Correspondence to: daihai.he@polyu.edu.hk (D.H.)

July 13, 2020

Abstract

Ebola virus disease (EVD) is a rare but fatal disease of humans and other primates caused by ebolaviruses. Study shows that the 2014-15 EVD outbreak causes more than 10,000 deaths. In this paper, we propose and analyze a deterministic model to study the transmission dynamics of EVD in Sierra Leone, Guinea, and Liberia. Our analyses show that the model has two equilibria: (1) the disease-free equilibrium (DFE) which is locally asymptotically stable (LAS) when the basic reproduction number ($\mathcal{R}_0$) is less than unity and unstable if it is greater than one, and (2) an endemic equilibrium (EE) which is globally asymptotically stable (GAS) when $\mathcal{R}_0$ is greater than unity. Furthermore, the backward bifurcation occurs, a co-existence between a stale DFE and a stable EE even if the $\mathcal{R}_0$ is less than unity, which makes the disease control more strenuous and would depend on the initial size of sub-population. By fitting to reported Ebola cases from Sierra Leone, Guinea, and Liberia in 2014-2015, our model has captured the epidemic patterns in all three countries and shed light on future Ebola control and prevention strategies.

Keywords: Ebola virus disease, mathematical modeling, bifurcation, stability analysis

1 Introduction

Ebola virus, also known as Ebola virus disease (EVD) (or Ebola hemorrhagic fever, denoted by EHF), is a viral hemorrhagic fever which is rare but highly fatal for humans and other primates. It is caused by ebolaviruses from the family of *Filoviridae* named after the village (river) where it was first identified [1, 2, 3, 4, 5]. The disease is a life-threatening infection that can be transmitted in population through direct contact with the EVD infected individual (either EVD sick person or dead body of EVD infected human) [4, 6, 5]. Evidences show that the disease can also be transmitted via sexual route between two partners of the same or different species [1, 7, 5]. The EVD is a serious threat to global public health and economics, especially, with the current rises of the disease outbreaks in Democratic Republic of Congo (DR Congo) with over 1500 deaths within three weeks by July 2019 [5, 8]. According to the World Health Organization (WHO), the EVD outbreaks mostly occur in West Africa, with the average case fatality rate (CFR) varying between 25% and 90% [5, 8].

The incubation period of EVD varies from 2-21 days (similar to Lassa fever disease) [4, 5]. Individuals infected with EVD cannot transmit the virus until signs and symptoms appear. The primary symptoms of EVD are fever, fatigue, muscle pain, headache, and sore throat, followed by the secondary symptoms (of severe cases) which include vomiting, diarrhea, skin rash, kidney, and liver malfunction, bleeding and so on [1, 2, 3, 4, 9, 10, 11, 12].

Although there is no specific vaccine against the virus, however, the rVSV-ZEBOV, which is still under clinical investigations, is the only one recommended by the World Health Organization (WHO). Preliminary data from WHO show that the rVSV-ZEBOV is highly effective and is currently in use since the 2018-2019 EVD outbreaks in DR Congo [2, 5]. So far there is yet no direct (licensed) treatment available for EVD. However, a range of some (effective) treatments including blood products, immune therapies, and drug therapies are currently being evaluated [5].

Numerous modeling studies of EVD have been carried out to explore the transmission dynamics of EVD in human population [1, 2, 3, 4, 6, 9, 10, 11, 12, 13, 14]. Chowell et al. [13] developed and analyzed a stochastic Susceptible-Exposed-Infectious-Recovered (SEIR) model to fit the EVD epidemics data in Congo and Uganda from 1995-2000. Their model was further extended in 2007 by Legrand et al. [14] by adding two essential classes, which are the hospitalized and the unburied dead body of infected individuals. In 2015, Weitz and Dushoff [6] formulated a model to study the effects of post-death transmission dynamics of EVD and to examine the inference problems and some opportunities for control measures. They showed that the parameters are unidentifiable and lead to underestimated basic reproduction number. Abbate et al. [1] designed a mathematical model to examine the potential impact of sexual transmission. Their analysis shows that the reduction of sexual activities and the use of condoms could decrease the sexual transmission rate. Though it may not necessarily reduce the epidemic size significantly, it would provide enough time for the preparation against the disease epidemic. In 2017, Agusto [2] developed and rigorously analyzed a model to describe the transmission dynamics of EVD by incorporating disease relapse and reinfection and found that the model with reinfection exhibits backward bifurcation phenomenon. This study also reveals a strong and positive correlation between key parameters (i.e., relapse and reinfection) and the total new cases, therefore suggests prioritizing the control measures on relapse and reinfection. Denes and Gumel [4] proposed a new deterministic model by including quarantine, and investigated the outbreaks in West Africa in 2014, they emphasized the effectiveness of quarantine in population-level.

Table 1: Pearson correlations between the epidemic weeks and geographic distances.

Direction	Correlation (95% CI)	p-value
Longitude	$0.474\ (0.156, 0.703)$	0.0054
Latitude	$0.715\ (0.483, 0.853)$	< 0.0001
Seashore	$0.614\ (0.357, 0.784)$	< 0.0001

In this study, we reference the aforementioned studies [1, 6], conduct spatial analysis, and explore the transmission dynamics of EVD in Sierra Leone, Guinea and Liberia between 2014 and 2015. We analyze and compare the transmission trends of EVD in these three countries during 2014-15 outbreaks. We divide the susceptible population into high-risk (those who are not vaccinated with rVSV-ZEBOV, or live in EVD high-risk endemic area) and low-risk (those who are vaccinated, or live in EVD low-risk endemic area). We also include the sexual route to explore its impacts on EVD transmission. We fit the model by using the plug-and-play inference framework [15]. Our simulation results offer insights into the patterns of EVD epidemics in Sierra Leone, Guinea, and Liberia during the 2014-15 outbreaks, as well as useful guidelines for the design of control and prevention strategies. This paper is organized as follows. The epidemic model is formulated and analyzed in section 2 and 3. In section 4, fitting results are obtained.

2 Data and methods

2.1 Data collection and spatial analysis

We obtained the weekly cases of Ebola virus disease (EVD), reported between Jan 2014 to Sept 2015, from 62 districts of the three hardest-hit West African countries (33 districts from Guinea, 14 from Sierra Leone and 15 from Liberia) from Ebola Situation Reports by the WHO. The district populations were obtained from [16], and also the boundaries of each district were obtained from the Database of Global Administrative Areas (also known as GADM maps and data) [17]. The weekly situation reports and patient reports for EVD are depicted in Fig. 1.

The epidemic week (EW) for the j-th region is the mean time of infection of all infected individuals over the course of the epidemic under investigation [18]. Thus, in the j-th region, there are n_i confirmations in the w_i-th week, so that

$$\mathrm{EW}_j = \sum_i n_i w_i / \sum_i n_i.$$

We calculated the correlation and p-value of the epidemic week in bins versus the geographic distance (in the units of longitude or latitude degrees) in three directions. The correlations and p-values are shown in Table 1.

In Fig. 2 (a), the greyscale area is used to show the population standardized cumulative cases in 62 districts. We project the 62 districts into 50 bins in three directions, i.e., longitude, latitude and along the seashore. Further, we calculate the average EW for each bin and statistical analyses are performed. The epidemic waves in these three directions are shown in panels (b-d) of Fig. 2, respectively.

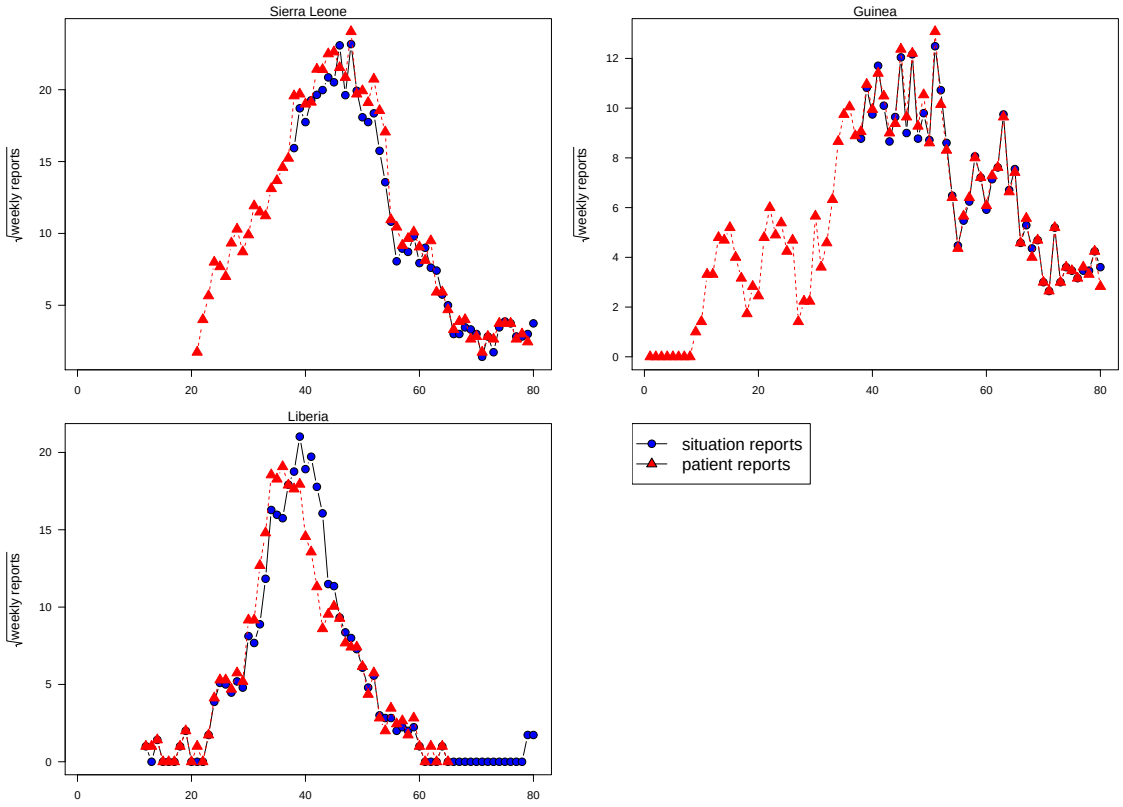

Figure 1: Data are obtained from WHO Ebola Situation Reports. These data are from two schemes from the three hardest-hit countries: situation reports and patient reports. Data from these two schemes are largely consistent, except for the peak in Liberia. When the data from both schemes are available, we use the average cases for fitting the models, otherwise, we use the available one, either from situation reports or from patient reports.

2.2 Model formulation

Let N be the total human population size, which is divided into six classes: (1) the high-risk susceptible individuals S_1, who are not vaccinated with rVSV-ZEBOV, or live in EVD high-risk endemic area, (2) the low-risk susceptible individuals S_2, who are vaccinated with rVSV-ZEBOV or live in EVD low-risk endemic area, (3) the exposed individuals E, (4) the infectious individuals I, (5) the recovered individuals R, and (6) the Ebola virus deceased individuals D.

The susceptible humans are recruited (by birth) at a rate π. A fraction (ρ) of total newly recruited humans joins S_1 and the remaining fraction $(1-\rho)$ joins S_2. Individuals in S_1 and S_2 are assumed to join E, by effective contacts with I at rates λ and $v\lambda$, respectively. Note that $0 \leq v \leq 1$. σ measures a progression rate from E to I. Individuals from I can recover or decease at a rate γ, a fraction f of which joins D (where f is the EVD induced death rate), while the remaining fraction of which joins R. θ measures the burial rate of the Ebola virus deceased individuals. β_c represents the non-sexual transmission rate (community and funeral), while β_s represents the sexual transmission rate of EVD. Furthermore, μ is the natural death rate of humans. We also assumed that there was no movement of

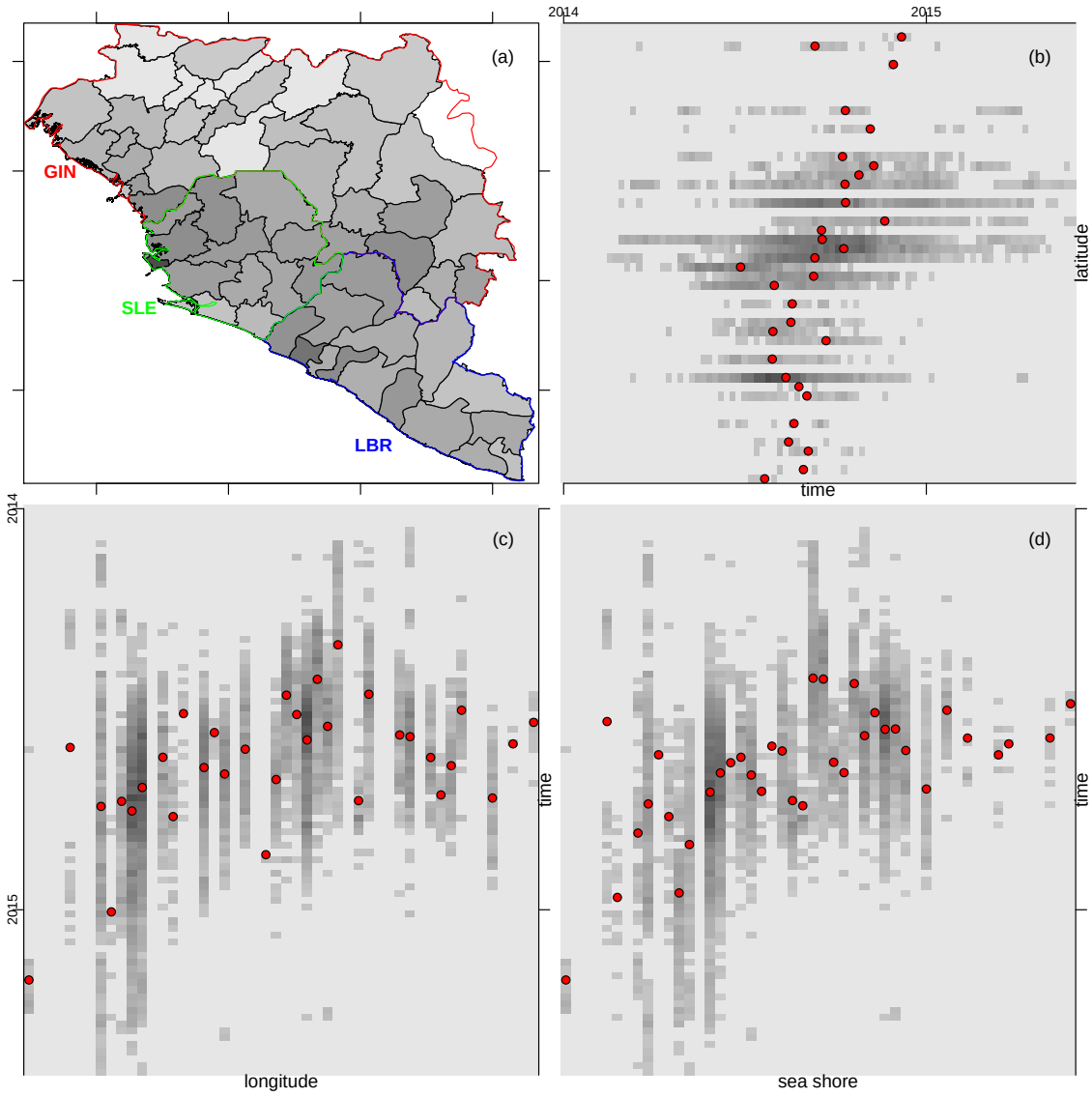

Figure 2: EVD spreading pattern. Panel (a) shows population standardized cumulative cases in greyscale. Panel (b) shows the wave of the epidemic along latitude. Panel (c) shows the wave of the epidemic along longitude. Panel (d) shows the wave of the epidemic along the seashore. Red bullet points are the epidemic week for the specified location.

individuals from S_1 to S_2 and *vice versa* during the outbreak.

The nonlinear system of ordinary differential equations below describes the transmission dynamics of EVD between two communities (i.e., high-risk and low-risk endemic areas). The flow diagram is depicted in Fig. 3. The state variables and parameters used in the model are summarized in Table 2.

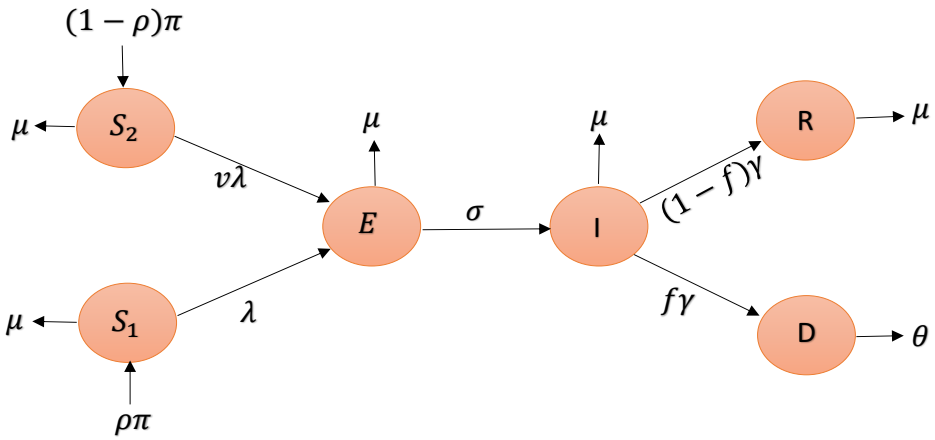

Figure 3: The schematic diagram of model (2.1).

$$\begin{aligned}
\frac{\mathrm{d}S_1}{\mathrm{d}t} &= \rho\pi - (\lambda+\mu)S_1,\\
\frac{\mathrm{d}S_2}{\mathrm{d}t} &= (1-\rho)\pi - (v\lambda+\mu)S_2,\\
\frac{\mathrm{d}E}{\mathrm{d}t} &= \lambda(S_1+vS_2) - (\sigma+\mu)E,\\
\frac{\mathrm{d}I}{\mathrm{d}t} &= \sigma E - (\gamma+\mu)I,\\
\frac{\mathrm{d}R}{\mathrm{d}t} &= (1-f)\gamma I - \mu R,\\
\frac{\mathrm{d}D}{\mathrm{d}t} &= f\gamma I - \theta D,
\end{aligned} \tag{2.1}$$

where the force of infection is given by $\lambda = \frac{(\beta_c+\beta_s)I+\beta_c\psi D}{N}$.

The total human population, N, at time t, is given by $N = S_1 + S_2 + E + I + R + D$. Therefore,

$$\frac{\mathrm{d}N}{\mathrm{d}t} = \pi - \mu N - \theta D \leq \pi - \mu N. \tag{2.2}$$

Obviously, one can show, by solving N in equation (2.2), that all solutions of the model starting in the region Ω remain in Ω for all $t \geq 0$. Thus, the region Ω is positive-invariant. Therefore, we consider all solutions restricted to Ω. In this region, we assumed that the usual existence, uniqueness, and continuation results hold for model (2.1) [19, 20].

Table 2: Description of the state variables and parameters of model (2.1)

	Description
Variable	
S_1	High-risk susceptible individuals
S_2	Low-risk susceptible individuals
E	Population of exposed humans
I	Population of infectious humans
R	Population of recovered humans
D	Ebola virus deceased individuals
Parameter	
π	Recruitment rate
β_c	Non-sexual (community and funeral) transmission rate
β_s	Sexual transmission rate
μ	Natural death rate
v	Rate of reduction in infectiousness from S_2
σ	Progression rate from E to I
γ	Recovery rate from infectious individuals
θ	Burial rate of Ebola virus deceased individuals
ρ	Fraction of newly recruited humans moving to S_1
ψ	Modification parameter for infectiousness
f	Fraction of symptomatic individuals who died from the disease
$1-f$	Fraction of symptomatic individuals who recovered from the disease

3 Mathematical analysis

3.1 Disease-free equilibrium

In the absence of the disease (i.e., $E = I = R = D = 0$), we obtained the disease-free equilibrium (DFE) of model (2.1) at steady state which is given by

$$\Gamma^0 = (S_1^0, S_2^0, E^0, I^0, R^0, D^0) = \left(\frac{\rho\pi}{\mu}, \frac{(1-\rho)\pi}{\mu}, 0, 0, 0, 0\right).$$

We employ the next generation matrix technique to compute the basic reproduction number of model (2.1), denoted by $\mathcal{R}_0 = \rho^*(FV^{-1})$, where ρ^* is the spectral radius of the next generation matrix (FV^{-1}), given in equation (3.2) [21, 22]. The matrices F (for the new infection terms) and V (for the remaining transition terms), associated with model (2.1) , are given, respectively, by:

$$F = \begin{bmatrix} 0 & (\beta_c+\beta_s)[\rho+(1-\rho)v] & \beta_c\psi[\rho+(1-\rho)v] \\ 0 & 0 & 0 \\ 0 & 0 & 0 \end{bmatrix}, \; V = \begin{bmatrix} g_1 & 0 & 0 \\ -\sigma & g_2 & 0 \\ 0 & -f\gamma & \theta \end{bmatrix}, \tag{3.1}$$

where $N^0 = \frac{\pi}{\mu}$, $S_1^0 = \frac{\rho\pi}{\mu}$, $S_2^0 = \frac{(1-\omega)\pi}{\mu}$, $g_1 = \sigma + \mu$, and $g_2 = \gamma + \mu$. Therefore, the basic reproduction

number, $\mathcal{R}_0$, is given by

$$\mathcal{R}_0 = \frac{[(\beta_c + \beta_s)\theta + f\gamma\psi\beta_c][(1-\rho)v + \rho]\sigma}{g_1 g_2 \theta}. \tag{3.2}$$

The basic reproduction number, $\mathcal{R}_0$, is defined as the average number generated by a single EVD infected individual in a fully susceptible population [20, 21, 23, 24]. The results below follow Theorem 2 of [21].

Theorem 3.1. *The DFE, Γ^0, of model (2.1), is locally-asymptotically stable (LAS) in Ω if $\mathcal{R}_0 < 1$, and unstable if $\mathcal{R}_0 > 1$.*

The epidemiological interpretation of $\mathcal{R}_0$ is that if $\mathcal{R}_0 < 1$, the EVD will die with time provided that the initial size of infected sub-populations of the system (2.1) is small so that the initial state of the system is in the basin of attraction of the DFE.

3.2 Endemic equilibrium

The Endemic Equilibrium (EE) of model (2.1) is the steady state where the disease may persist in the community, i.e., when at least one of the infected compartments is non-empty. Let $\Gamma^* = (S_1^*, S_2^*, E^*, I^*, R^*, D^*)$ be the EE for the system (2.1). Therefore, the EE in terms of λ^* (i.e., force of infection) is given by

$$\begin{aligned}
S_1^* &= \frac{\pi\rho}{\lambda+\mu}, \\
S_2^* &= \frac{\pi(1-\rho)}{\lambda v+\mu}, \\
E^* &= \frac{\pi\lambda[(1-\rho)v\lambda + (1-\rho)v\mu + \rho v\lambda + \rho\mu]}{g_1(\lambda v+\mu)(\lambda+\mu)}, \\
I^* &= \frac{\pi\lambda\sigma[(1-\rho)v\lambda + (1-\rho)v\mu + \rho v\lambda + \rho\mu]}{g_1 g_2(\lambda v+\mu)(\lambda+\mu)}, \\
R^* &= \frac{(1-f)\gamma\pi\sigma\lambda[(1-\rho)v\lambda + (1-\rho)\mu v + \rho v\lambda + \rho\mu]}{\mu g_1 g_2(\lambda v+\mu)(\lambda+\mu)}, \\
D^* &= \frac{f\gamma\pi\sigma\lambda[(1-\rho)v\lambda + (1-\rho)\mu v + \rho v\lambda + \mu\rho]}{\theta g_1 g_2(\lambda v+\mu)(\lambda+\mu)},
\end{aligned} \tag{3.3}$$

where,

$$\lambda^* = \frac{(\beta_c + \beta_s)I^* + \beta_c\psi D^*}{N^*}, \tag{3.4}$$

and

$$N^* = S_1^* + S_2^* + E^* + I^* + R^* + D^*. \tag{3.5}$$

Therefore, equation (3.5) can now be written as

$$S_1^* + S_2^* + E^* + \left(1 - \frac{(\beta_c+\beta_s)}{\lambda^*}\right)I^* + R^* + \left(1 - \frac{\beta_c\psi}{\lambda^*}\right)D^* = 0. \tag{3.6}$$

Hence, we obtain the EE of the system (2.1) which corresponds to (positive) solutions of the equation (3.6).

Table 3: Descriptions of the parameters in model (2.1)

Parameter	Value (Range)	Units/Remarks	Sources
π	400	Person·day^{-1}	[2]
β_c	0.3045	Day^{-1}	[2]
β_s	0.001 (0.0005 – 0.002)	Day^{-1}	Estimated, [1]
μ	0.00004	Day^{-1}	[2]
v	0.045	Day^{-1}	Assumed
δ	0.1139	Day^{-1}	[4]
σ	0.5239	Day^{-1}	[2]
γ	0.5366	Day^{-1}	[2]
θ	0.5	Day^{-1}	[2]
ρ	0.75	Day^{-1}	Assumed
f	0.48	Day^{-1}	[2]
ψ	0.21	Day^{-1}	[2]

3.3 Bifurcation analysis

The backward bifurcation (BB) phenomenon indicates that the requirement $\mathcal{R}_0 < 1$, is though necessary, not sufficient for effective epidemic control. This phenomenon has been studied in numerous mathematical modeling studies [20, 25, 26, 27, 28, 29, 30]. The BB analysis for the model (2.1) will be explored in the next sub-section.

3.3.1 Existence of endemic equilibria and backward bifurcation

Following the existence of the EE in section 3.2, we substitute equation (3.3) into equation (3.6) and simplify, then the following quadratic equation (in terms of λ^*) is obtained

$$a_1\lambda^{*2} + a_2\lambda^* + a_3 = 0, \tag{3.7}$$

where

$$\begin{aligned}
a_1 =&((v(g_2+\sigma)\theta + fv\gamma\,\sigma)\mu + v\gamma\sigma\theta(1-f))\pi,\\
a_2 =&((-((-1+\rho)v-\rho)(g_2+\sigma)\theta - \gamma((-1+\rho)v-\rho)f\sigma)\mu^2 + ((((\gamma(-1+f)\rho + (1-f)\gamma - \beta_c - \beta_s)v\\
&- \gamma(-1+f)\rho)\sigma + g_1g_2(\rho v - \rho + 1))\theta - fv\gamma\sigma\beta_c\psi)\mu)\pi, \text{ and } a_3 = \mu^2\pi\theta g_1 g_2(1-\mathcal{R}_0).
\end{aligned}$$

Obviously, from equation (3.7), one can compute the solutions of the EE, by substituting only the positive values of λ_h into equation (3.3). Therefore, the existence of the quadratic equation (3.7) highlights the existence of BB for the model (2.1). Hence, we obtain the following results.

Theorem 3.2. *The model (3.1) has:*

i. a unique endemic equilibrium if $a_3 < 0$ *or* $\mathcal{R}_0 > 1$,

ii. a unique endemic equilibrium if $a_2 < 0$ *and* $a_3 = 0$,

iii. two endemic equilibria if $a_2 < 0$, $a_3 > 0$ *and* $\Delta > 0$,

iv. no endemic equilibrium otherwise.

Clearly, case (i) of Theorem 3.2 indicates that the model (2.1) has a unique EE whenever $\mathcal{R}_0 < 1$. Furthermore, Case (iii) highlights the possibility of the existence of BB. In BB setting, the LAS DFE co-exists with a LAS EE whenever $\mathcal{R}_0 < 1$ in the model (2.1) [20, 25, 26, 27, 28]. To verify, we let the discriminant $a_2^2 - 4a_1a_3 = 0$ and simplify for the critical value of $\mathcal{R}_0$, denoted by $\mathcal{R}_0^c$ and given by

$$\mathcal{R}_0^c = 1 - \frac{a_2^2}{4a_1\mu^2\pi\theta g_1 g_2}. \tag{3.8}$$

Hence, the BB would occur for values of $\mathcal{R}_0$ such that $\mathcal{R}_0^c < \mathcal{R}_0 < 1$. The BB curve is depicted in Fig. 4. The parameters used can be found in Table 3, with $\beta_c = 0.5$, $\beta_s = 0.0201$, $v = 1.45$, $\gamma = 0.69$, $\theta = 0.75$, $\rho = 0.0075$ and $f = 0.948$ (see Table 3 for the units of the aforementioned parameters) chosen for illustrative purpose. Hence, $\mathcal{R}_0^c = 0.8592612498 < 1$ and $\mathcal{R}_0 = 0.8863690533 < 1$, so that the inequality $\mathcal{R}_0^c < \mathcal{R}_0 < 1$ is satisfied.

Thus, the following result is established.

Lemma 3.3. *The model* (2.1) *undergoes the phenomenon of BB when Case (iii) of the Theorem 3.2 holds and* $\mathcal{R}_0^c < \mathcal{R}_0 < 1$.

The epidemiological implications of the existence of BB in EVD is that the classical requirements of having $\mathcal{R}_0 < 1$ is no longer sufficient (although necessary) for effectively controlling EVD. Therefore, disease elimination would depend on the initial sizes of sub-populations of the systems (2.1) [2, 20, 25, 26, 27, 28, 29, 31].

Corollary 3.4. *The model* (2.1) *does not undergo backward bifurcation phenomena if* $v = 0$.

Here, we set the parameter $v = 0$ (i.e., rate of reduction in infectiousness from the low-risk susceptible individuals) and all other parameter values remain as used for the BB analysis and Table 3. In this case, the basic reproduction number can be written as $\mathcal{R}_0^n = \frac{[(\beta_c+\beta_s)\theta+f\gamma\psi\beta_c]\rho\sigma}{g_1 g_2\theta} < 1$. Thus, the model (2.1) admits a unique stable DFE as in line with Theorem 3.1. In addition, the DFE is locally asymptotically stable (LAS) whereas the EE is unstable if $\mathcal{R}_0^n < 1$ (see Theorem 3.1). Therefore, the coefficient of the quadratic equation (3.7), that is a_1, a_2, and a_3, are now given by $a_1 = 0$, $a_2 = ((\rho\,(g_2+\sigma)\,\theta + \rho\,f\gamma\,\sigma)\,\mu^2 + (-\gamma\,(f-1)\,\rho\,\sigma + g_1g_2\,(1-\rho))\,\theta\,\mu)\,\pi$, and $a_3 = \mu^2\pi\theta g_1 g_2(1-\mathcal{R}_0^n)$.

Thus, following Theorem 3.2, there is no EE when $\mathcal{R}_0^n \leq 1$. Because the quadratic equation (3.7) will become linear, i.e., $\lambda^n = \frac{-a_3}{a_2}$ indicating that the model (2.1) has no EE whenever $\mathcal{R}_0^n \leq 1$. Hence, the analysis shows that the parameter v causes the existence of the BB for the model (2.1), and this parameter is related to the compartment of low-risk susceptible individuals or vaccinated individuals.

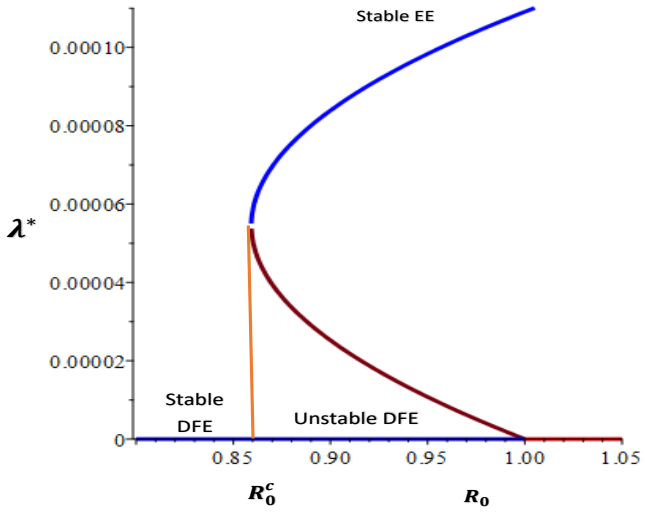

Figure 4: Backward bifurcation curve of the model (2.1). The parameters used can be found in Table 3, with $\beta_c = 0.5$, $\beta_s = 0.0201$, $v = 1.45$, $\gamma = 0.69$, $\theta = 0.75$, $\rho = 0.0075$ and $f = 0.948$, so that, $\mathcal{R}_0^c = 0.8592612498 < \mathcal{R}_0 = 0.8863690533 < 1$.

3.3.2 Global stability analysis of the endemic equilibrium

Following the previous works [26, 29, 32, 33], the following Theorem 3.5 is established.

Theorem 3.5. *The endemic equilibrium point (EE) of the model (2.1), E^*, is globally-asymptotically stable (GAS) in the region of attraction, Ω^0, whenever $\mathcal{R}_0 > 1$, provided that*

$$\left(1 - \frac{\lambda}{\lambda^*}\right)\left(1 - \frac{I\lambda^*}{I^*\lambda}\right) \geq 0 \tag{3.9}$$

and

$$\left(1 - \frac{\lambda}{\lambda^*}\right)\left(1 - \frac{D\lambda^*}{D^*\lambda}\right) \geq 0 \tag{3.10}$$

are satisfied.

For the proof of the above theorem, see Appendix (A1).

4 Simulations and model fittings

4.1 Simulations

To explore the impact of the reduction in infectiousness and the newly recruitment rate on the dynamical system described in equation (2.1), we conducted simple simulations, with multiple choices

of these two parameters. The simulation results in Fig. 5 is in line with our theoretical analyses in Section 3, indicating that the rate of reduction in infectiousness from the low-risk susceptible individuals or vaccinated individuals (i.e., v) is the cause of the occurrence of backward bifurcation. In other word, it emphasizes the significance of vaccination as the potential strategy in combating the EVD in the endemic areas.

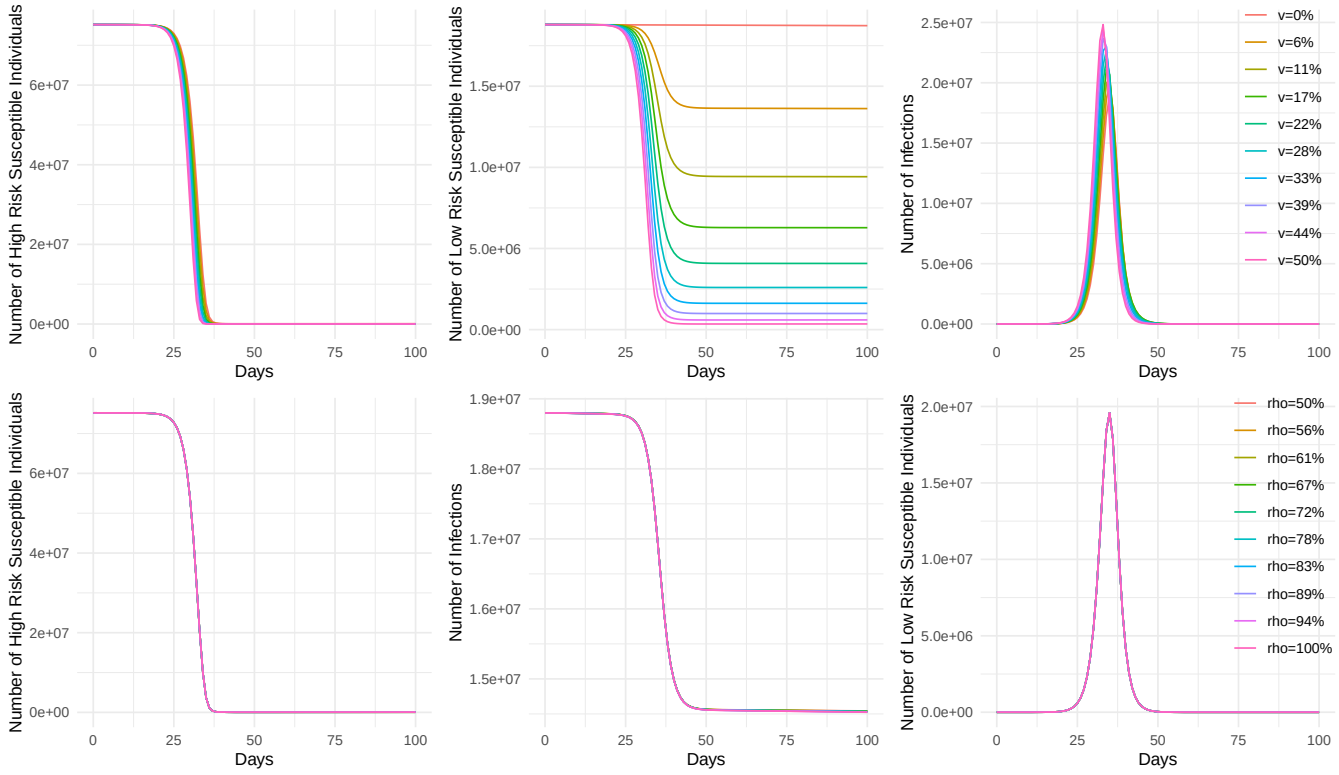

Figure 5: Simulation changes of the number of high-risk susceptible individuals, low-risk susceptible, and infections in (2.1) with different choices of rate of reduction (v) and newly recruitment (ρ). Parameters are same as those in Table 3, except $\beta_c = 3.045$. Initial populations are set as $N_0 = 1e^8$, $I_0 = 10$, $R_0 = 0.06N$, $D_0 = 0$, $S_0 = N_0 - I_0 - R_0 - D_0$. The initial ratio between S_1 and S_2 is 4:1.

4.2 Fitting framework

In this section, we employed the plug-and-play inference framework for fittings the model to real data [15]. The analyses in this section will be carried out for a special scenario of the model (2.1) (in close domain) by lumping the high-risk and low-risk susceptible individuals into one compartment (i.e., $S = S_1 + S_2$), we also assumed that the non-sexual transmission rate is coupled with sexual transmission rate, and is given by $\beta_c + \beta_s = \beta$. We further set the birth and death rate to be zero each (i.e., $\pi = \mu = 0$), meaning that there is no birth and natural death within a short period of time, and also the Ebola-induced mortality rate is zero ($\delta = 0$). The reduced model is similar to the model proposed by Weitz and Dushoff in [6]. Therefore, the simplified version of the model (2.1) together with the above assumptions is given by

$$
\begin{aligned}
\frac{\mathrm{d}S}{\mathrm{d}t} &= -(\beta I + \psi D)\frac{S}{N}, \\
\frac{\mathrm{d}E}{\mathrm{d}t} &= (\beta I + \psi D)\frac{S}{N} - \sigma E, \\
\frac{\mathrm{d}I}{\mathrm{d}t} &= \sigma E - \gamma I, \\
\frac{\mathrm{d}R}{\mathrm{d}t} &= (1-f)\gamma I, \\
\frac{\mathrm{d}D}{\mathrm{d}t} &= f\gamma I - \theta D.
\end{aligned} \tag{5.1}
$$

The basic reproduction number of the simplified model (5.1) is now given by $\mathcal{R}_0(t) = \frac{f\psi}{\theta} + \frac{\beta}{\gamma}$.

The number of EVD cases of the i-th week is given by

$$
Z_i = \int_{\text{week } i} \rho^* \gamma I \, \mathrm{d}t, \tag{5.2}
$$

where ρ^* represent a constant reporting rate of EVD cases.

Partially Observed Markov Process (POMP), also known as Hidden Markov Model (HMM), is employed to model the EVD weekly reported cases (C_i, where i denotes the week during the study period). The observed weekly number of EVD confirmed cases, given by C_i, is a random sample from a negative-binomial (NB) distribution, assuming the rate of the Poisson distribution is a Gamma random variable. Hence, for each (or a single) year, we have

$$
C_i \sim \text{NB}(\text{mean} = Z_i, \text{variance} = Z_i(1 + \xi Z_i)), \tag{5.3}
$$

where ξ represents an over-dispersion parameter for NB distribution to be estimated. Note that $\xi > 0$. Hence, we set $L_i(\cdot)$ to be the likelihood function for the i-th week during the study period, which measures the probability of the observed weekly number of EVD cases, given the real cases from Z_i under the NB distribution in Eqn (5.3) [15, 34]. We employed the `R` (version 3.4.1) package "`POMP`" [35] for the model fittings.

The overall log-likelihood, l, for all the time series is given by

$$
l(\Theta) = \sum_{i=1}^{T} \ln[L_i(C_i \mid C_0, ..., C_{i-1}; \Theta)], \tag{5.4}
$$

where Θ denote the parameter vector under estimation, and T measure the total number of weeks in a wave.

Further, we applied the iterated filtering algorithm within the plug-and-play likelihood-based inference framework to obtain the maximum likelihood estimates (MLE) of Θ ([34, 36, 37, 38, 39, 40, 41]. We used the fixed-time-step Euler-multinomial algorithm to simulate the model (2.1). We compared the performance of each model using the small-sample-size corrected Akaike's Information Criterion (AICc) [42]. The AICc measure the trade-off between the model complexity and the goodness-of-fit, and is given by

$$\text{AICc} = -2l\left(\hat{\Theta}\right) + 2k + \frac{2Y_2(Y_2+1)}{Y_1 - Y_2 - 1}, \tag{5.5}$$

where Y_1 denote the number of data points, i.e., sample size, and Y_2 represent the number of parameters to be estimated.

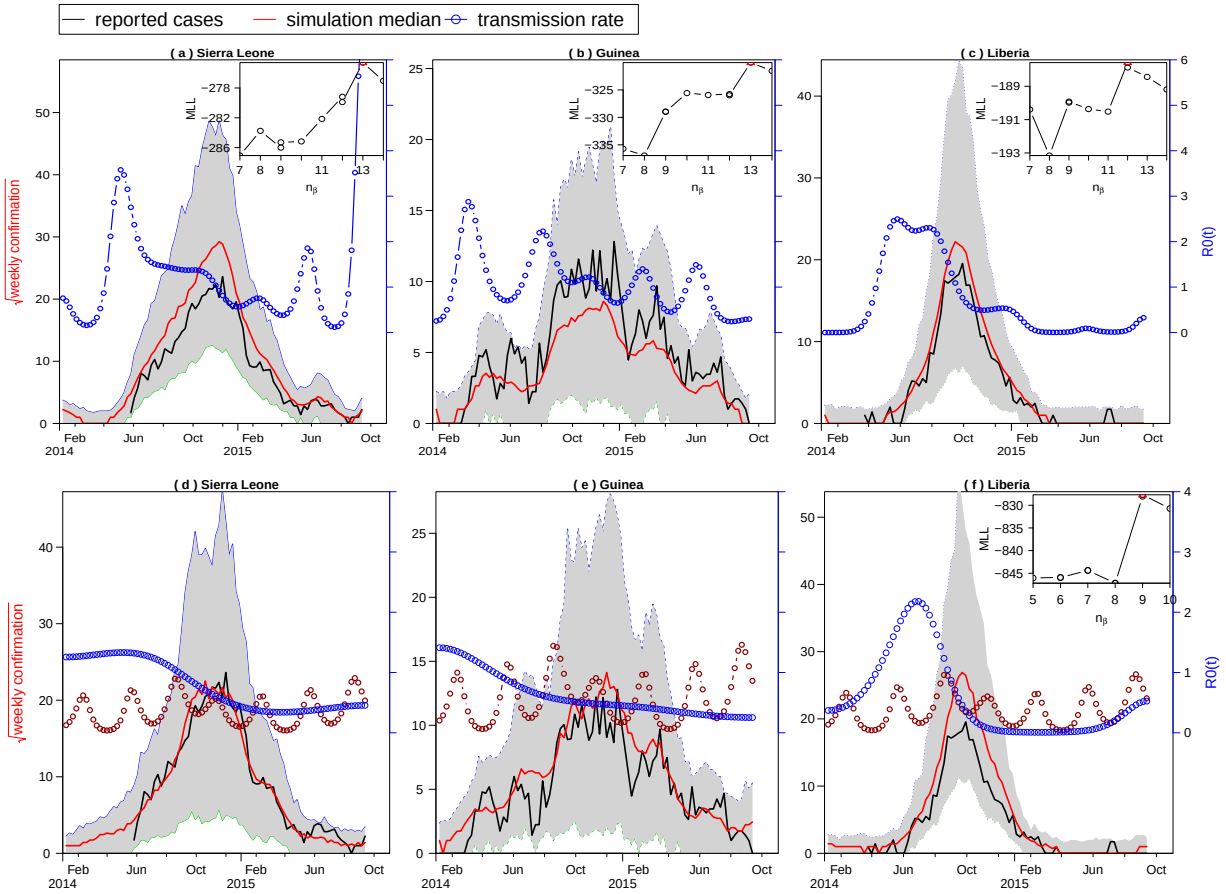

Figure 6: Model fitting results. Panels (a-c) with secular change only (no periodic component), realized as a flexible cubic spline with n_β nodes: red curve as median of 1000 simulations, blue circled curve as the estimated transmission rate. Panels (d-f) with different secular trend (a spline function with four nodes) for each country and a common periodic component (a periodic spline with n nodes) for the three countries in the transmission rate: blue circled curve as the secular trend while brown circled curve as the common periodic component. Inset panel shows the profile maximum log likelihood as a function of the number of nodes in the transmission rate (a-c) or in the periodic component (d-f).

4.3 Fitting results

Here, the epidemic model (5.1) was fitted by using either seasonally periodic or non-periodic forcing or a combination of the two, to the EVD laboratory confirmed cases from Jan 2014 to Sept 2015 for Sierra Leone, Guinea, and Liberia. According to the recent work of Weitz and Dushof [6], we used the following values of parameters: $\sigma^{-1} = 11$ days (mean latent period), $\gamma^{-1} = 6$ days (mean infectious period), $\theta^{-1} = 4$ days (mean duration of post-death infection), $f = 0.7$ (case fatality ratio), $\psi = 0.25$ (so that $1 - \psi = 0.75$). The estimated population size for the three countries during the study period obtained from the World Bank are as follows: 6,092,000 for Sierra Leone, 11,750,000 for Guinea, and 4,294,500 for Liberia [43]. In addition, we allowed the transmission rate to be time varying, in particular, we used the cubic spline function, and we denoted the values of the node as n_{β_i}, $i = 1, ..., n$. In Fig. 6 panel (a-f), we considered two different models: a non-periodically forced model, without periodic component in the transmission rate (a-c); and a combination of two types of transmission, namely, a common periodic forcing with a secular trend (fixed 4 nodes) in the transmission rate (d-f). We calculated the profile log likelihood of the three models for the three countries as a function of the number of nodes in the transmission rate n_β. Fig. 6 panel (d-f) reveals a periodic component consisting of multiple waves during the fitting period. This periodic component could reflect: (i) human behavioral reaction, (ii) holidays, market and school terms. Meanwhile, from both panel (a-c) and panel (d-f), reasonable difference is observed from their secular trends among the three hardest-hit countries, which probably implies the inconsistent control measure of these three countries.

In Table 4, the non-periodic model outperforms the combined model in the three countries, with smaller AICc. It should be noted that $\mathcal{R}_0^*$ in the non-periodic model for Liberia is 0.98, smaller than one, which indicates that the EVD outbreaks in Liberia had been significantly curbed or reduced by September 2015.

Table 4: Summary of the model fitting performance.

	Non-periodic			Combined		
Country	AICc	$\mathcal{R}_0^*$	$S(0)$	AICc	$\mathcal{R}_0^*$	$S(0)$
Sierra Leone	552.8	2.39	0.51	566.7	1.23	0.94
Guinea	643.1	1.46	0.83	656.7	1.21	0.93
Liberia	400.2	0.98	0.89	406.1	1.13	0.94

5 Discussion

We developed and analyzed a model to explore the transmission dynamics of Ebola virus disease in Guinea, Sierra Leone, and Liberia between 2014 and 2015. We showed that the model (2.1) has two equilibria, of which the disease-free equilibrium (DFE) is locally asymptotically stable (LAS) when the basic reproduction number ($\mathcal{R}_0$) is less than one, and unstable if it is greater than one ($\mathcal{R}_0 > 1$). We also showed that the endemic equilibrium (a situation where the disease persist to the community) is globally asymptotically stable (GAS) when the basic reproduction number is greater than one ($\mathcal{R}_0 > 1$). Further analysis reveals that the backward bifurcation (BB) phenomenon would occur for values of $\mathcal{R}_0$ such that $\mathcal{R}_0^c < \mathcal{R}_0 < 1$. In a backward bifurcation setting, the classical requirements of having

$\mathcal{R}_0 < 1$ is no longer sufficient (although necessary) for effectively controlling the Ebola virus disease. Therefore, disease elimination would depend on the initial size of the sub-populations of the model (2.1) [2, 20, 25, 26, 27, 28, 29, 31]. Our analytical results also suggested that the backward bifurcation can be removed when the rate of reduction in infectiousness from the low-risk susceptible individuals, or when the basic reproduction number is equal to one, reflecting the significance of vaccination as the potential strategy in controlling EVD in the endemic areas. We note that the vaccination part is to evaluate a hypothetical situation based on the past outbreak of Ebola virus disease in 2014-15. In reality, the vaccine was not in use in 2014-15 outbreaks.

We performed model simulations to highlight the impact of reduction in infectiousness and the newly recruitment rate on the model. Our simulations reveal that the rate of reduction in infectiousness and newly recruitment parameter are the keys to lead to the existence of backward bifurcation for our model. The plug-and-play statistical inference framework on the special scenario of the model (2.1) (in a close domain) was used for fitting the real cases of the Ebola virus disease in the three countries (i.e., Guinea, Sierra Leone, and Liberia) between 2014 and 2015. The model (5.1) was fitted well to the weekly reported cases in the three countries in 2014-15.

The reduced model (i.e., system (5.1)) identified a spreading wave of the Ebola virus disease from southeast to northwest along the seashore. Non-periodic and periodic patterns are used to reconstruct the transmission rate through time in these three countries. We found that the transmission rates were high at the beginning of each epidemic in all the three countries. In addition, we found that the transmission rate reduced gradually and maintained at low level in Liberia, where the Ebola virus disease was significantly controlled. Further, we showed that the model with exclusively non-seasonal transmission rate surpasses the model with combination of non seasonal transmission and periodic factors, indicating that, although there could be seasonal factors (e.g., climate or school terms), the secular variation, such as governmental control measures, played a key role in obtaining this kind of transmission pattern. Finally, our model was able to capture numerous dynamics properties of EVD within the three countries, even though some features were not captured (such as comparative analysis of Ebola virus disease epidemics in the three countries) due to the insufficiency of the data especially for the vaccinated people (low-risk susceptible individuals). This part is left for future work when the data becomes fully and publicly available.

Declarations

Ethics approval and consent to participate Since no personal data was collected, neither ethical approval nor individual consent was applicable.

Availability of data and materials The Ebola cases surveillance data used in this work were freely obtained via the public domains. The data may also be available based on request.

Funding This work was not funded.

Acknowledgements The authors are grateful to the handling editor and unanimous reviewers for their insightful and constructive comments which were used to improve the manuscript significantly.

Disclaimer The funding agencies had no role in the design and conduct of the study; collection, management, analysis, and interpretation of the data; preparation, review, or approval of the manuscript; or decision to submit the manuscript for publication.

Conflict of Interests The authors declared that they have no competing interests.

Authors' Contributions All authors contributed equally and gave final approval for publication of the manuscript.

References

[1] Abbate JL, Murall CL, Richner H, Althaus CL. Potential Impact of Sexual Transmission on Ebola Virus Epidemiology: Sierra Leone as a Case Study. PLoS Negl Trop Dis. 2016;10(5):e0004676.

[2] Agusto FB. Mathematical model of Ebola transmission dynamics with relapse and reinfection. Math Biosci. 2017;283:48–59. Available from: https://doi.org/10.1016/j.mbs.2016.11.002.

[3] Agusto FB, Teboh-Ewungkem MI, Gumel AB. Mathematical assessment of the effect of traditional beliefs and customs on the transmission dynamics of the 2014 Ebola outbreaks. BMC Medicine. 2015;13(96):318–3.

[4] Dénes A, Gumel AB. Modeling the impact of quarantine during an outbreak of Ebola virus disease. Infect Dis Model. 2019;4:12–27.

[5] Organization WH. Ebola virus disease - Democratic Republic of the Congo. 2019;Accessed July 2019. Available from: https://www.who.int/news-room/fact-sheets/detail/ebola-virus-disease.

[6] Weitz JS, Dushoff J. Modeling Post-death Transmission of Ebola: Challenges for Inference and Opportunities for Control. Sci Reports. 2015;5:8751.

[7] Luo D, Zheng R, Wang D, Zhang X, Yin Y, Wang K, et al. Effect of sexual transmission on the West Africa Ebola outbreak in 2014: a mathematical modelling study. Sci Reports. 2019;9:1653.

[8] Organization WH. Ebola virus disease - Democratic Republic of the Congo. 2019;Accessed July 2019. Available from: https://www.who.int/csr/don/11-july-2019-ebola-drc/en/.

[9] Barbarossa MV, Dénes A, Kiss G, Nakata Y, Röst G, Vizi Z. Transmission Dynamics and Final Epidemic Size of Ebola Virus Disease Outbreaks with Varying Interventions. PLoS ONE. 2015;10(7):e0131398.

[10] Kabli K, El Moujaddid S, Niri K, Tridane A. Cooperative system analysis of the Ebola virus epidemic model. Infect Dis Model. 2018;3:145–159.

[11] Kiskowski M, Chowell G. Modeling household and community transmission of Ebola virus disease: epidemic growth, spatial dynamics and insights for epidemic control. Virulence. 2015;7(2):163–173.

[12] Xie Z. Data Fitting and Scenario Analysis of Vaccination in the 2014 Ebola Outbreak in Liberia. Osong Public Health Res Perspect. 2019;10(3):187–201.

[13] Chowell G, Hengartner NW, Castillo-Chavez C, Fenimore PW, Hyman JM. The basic reproductive number of Ebola and the effects of public health measures: The cases of Congo and Uganda. J Theoret Biol. 2004;229(1):119e126.

[14] Legrand J, Grais RF, Boelle PY, Valleron AJ, Flahault A. Understanding the dynamics of Ebola epidemics. Epidemiol Infect. 2007;135(4):610–621.

[15] Breto C, He D, Ionides EL, et al. Time series analysis via mechanistic models. Ann Appl Stat. 2009;3:319–348.

[16] GeoHive - Spatial data made easy; 2019. Accessed July 2019. Available from: https://geohive.ie/.

[17] ADM maps and data; 2019. Accessed July 2019. Available from: https://gadm.org/.

[18] Brian SF, Viboud C, Koelle K, Ferrari MJ, Bharti N, Grenfell BT. Global Patterns in Seasonal Activity of Influenza A/H3N2, A/H1N1, and B from 1997 to 2005: Viral Coexistence and Latitudinal Gradients. PLOS ONE. 2007;12:e1296.

[19] Hussaini N, Okuneye K, Gumel AB. Mathematical analysis of a model for zoonotic visceral leishmaniasis. Infect Dis Model. 2017;2(4):455–474.

[20] Musa SS, Zhao S, Chan HS, Jin Z, He D. A mathematical model to study the 2014-2015 large-scale dengue epidemics in Kaohsiung and Tainan cities in Taiwan, China. Math Biosci Eng. 2019;16:3841–3863.

[21] Van-den Driessche P, Watmough J. Reproduction numbers and sub-threshold endemic equilibria for compartmental models of disease transmission. Math Biosci. 2002;180(1):29–48.

[22] Shuai Z, van den Driessche P. Global stability of infectious disease models using Lyapunov functions. SIAM J Appl Math. 2013;73(4):1513–1532.

[23] He D, Wang X, Gao D, Wang J. Modeling the 2016-2017 Yemen cholera outbreak with the impact of limited medical resources. J Theoret Biol. 2018;451:80–85.

[24] Zhao S, Stone L, Gao D, He D. Modelling the large-scale yellow fever outbreak in Luanda, Angola, and the impact of vaccination. PLoS Negl Trop Dis. 2018;12(1):e0006158.

[25] Anguelov R, Garba SM, Usaini S. Backward bifurcation analysis of epidemiological model with partial immunity. Comp Math Appl. 2014;68:931–940.

[26] Garba SM, Gumel AB, Mra B. Backward bifurcations in dengue transmission dynamics. Math Biosci. 2008;215(1):11–25.

[27] Gumel AB. Causes of backward bifurcations in some epidemiological models. J Math Anal Appl. 2012;395:355–365.

[28] Okuneye K, Gumel AB. Analysis of a temperature- and rainfall-dependent model for malaria transmission dynamics. Math Biosci. 2016;287:72–92.

[29] Roop-O P, Chinviriyasit W, Chinviriyasit S. The effect of incidence function in backward bifurcation for malaria model with temporary immunity. Math Biosci. 2015;265:47–64.

[30] Yang C, Wang X, Gao D, Wang J. Impact of awareness programs on cholera dynamics: two modeling approaches. Bull Math Biol. 2017;79(9):2109–31.

[31] Musa SS, Hussaini N, Zhao S, He D. Dynamical analysis of chikungunya and dengue co-infection model. Disc Cont Dyn Syst - B. 2019;22(11):1–27.

[32] Musa SS, Zhao S, Hussaini N, Habib AG, He D. Mathematical modeling and analysis of Meningococcal Meningitis transmission dynamics. Int J Biomath. 2020;13(1):2050006.

[33] Sun G, Xie J, Huang S, Jin Z, Li M, Liu L. Transmission dynamics of cholera: Mathematical modeling and control strategies. Commun Nonlinear Sci Numer Simulat. 2017;45:235–244.

[34] Lin Q, Lin Z, Chiu APY, et al. Seasonality of influenza A(H7N9) virus in China - fitting simple epidemic models to human cases. PLoS One. 2016;11:e0151333.

[35] The website of `R` package "`pomp`": statistical inference for partially-observed Markov processes;. Available from: https://kingaa.github.io/pomp/.

[36] Earn DJ, He D, Loeb MB, et al. Effects of school closure on incidence of pandemic influenza in Alberta, Canada. Ann Intern Med. 2012;156:173–181. Available from: http://annals.org/aim/article-abstract/1033342.

[37] He D, Dushoff J, Day T, et al. Mechanistic modelling of the three waves of the 1918 influenza pandemic. Theor Ecol. 2011;4(2):283–288.

[38] He D, Ionides EL, King AA. Plug-and-play inference for disease dynamics: measles in large and small populations as a case study. J Royal Soc Interf. 2010;7:271–283.

[39] He D, Lui R, Wang L, et al. Global Spatio-temporal Patterns of influenza in the post-pandemic era. Sci Rep;5:11013.

[40] Ionides EL, Bhadra A, Atchade Y, et al. Iterated filtering. Ann Stat. 2011;39:1776–1802.

[41] Ionides EL, Breto C, King AA. Inference for nonlinear dynamical systems. Proc Natl Acad Sci. 2006;103:18438–18443.

[42] Camacho A, Ballesteros S, Graham AL, Carrat F, Ratmann O, Cazelles B. Explaining rapid reinfections in multiple-wave influenza outbreaks: Tristan da Cunha 1971 epidemic as a case study. Proc Biol Sci. 2011;278:3635–3643. Available from: https://doi.org/10.1098/rspb.2011.0300.

[43] Data WB. Population website. 2019;Accessed January 2019. Available from: https://data.worldbank.org/indicator/SP.POP.TOTL?locations=NG.

[44] LaSalle JP. The stability of dynamical systems, Regional Conference Series in Applied Mathematics. SIAM Philadelphia; 1976.

Appendices

A1 The Proof of Theorem 3.5 using direct Lyapunov function theory

Proof. Here, we adopt previous technique to prove Theorem 3.5 (see, for instance [29, 33, 30]). Firstly, we define a Lyapunov function given below:

$$\begin{aligned} V(t) =& n_1\left(S_1 - S_1^* - S_1^* \ln\frac{S_1}{S_1^*}\right) + n_2\left(S_2 - S_2^* - S_2^* \ln\frac{S_2}{S_2^*}\right) + n_3\left(E - E^* - E^* \ln\frac{E}{E^*}\right) + \\ & n_4\left(I - I^* - I^* \ln\frac{I}{I^*}\right) + n_5\left(D - D^* - D^* \ln\frac{D}{D^*}\right). \end{aligned} \tag{A-1}$$

Therefore, the derivative of the Lyapunov function (A-1) calculated along solutions of the model (2.1) is given by

$$\dot{V}(t) = n_1\left(1 - \frac{S_1^*}{S_1}\right)\dot{S}_1 + n_2\left(1 - \frac{S_2^*}{S_2}\right)\dot{S}_2 + n_3\left(1 - \frac{E^*}{E}\right)\dot{E} + n_4\left(1 - \frac{I^*}{I}\right)\dot{I} + n_5\left(1 - \frac{D^*}{D}\right)\dot{D}. \tag{A-2}$$

By direct computation from equation (A-2), we have

$$\begin{aligned} n_1\left(1 - \frac{S_1^*}{S_1}\right)\dot{S}_1 &= \left(1 - \frac{S_1^*}{S_1}\right)\left(\rho\pi - \lambda S_1 - \mu S_1\right) \\ &= n_1\left(1 - \frac{S_1^*}{S_1}\right)\left(\lambda^* S_1^* + \mu S_1^* - \lambda S_1 - \mu S_1\right) \\ &= n_1\lambda^* S_1^*\left(1 - \frac{S_1^*}{S_1}\right)\left(1 - \frac{\lambda S_1}{\lambda^* S_1^*}\right) - \mu\frac{(S_1 - S_1^*)^2}{S_1} \\ &\leq n_1\lambda^* S_1^*\left(1 - \frac{\lambda S_1}{\lambda^* S_1^*} - \frac{S_1^*}{S_1} + \frac{\lambda}{\lambda^*}\right), \end{aligned} \tag{A-3}$$

and,

$$\begin{aligned} n_2\left(1 - \frac{S_2^*}{S_2}\right)\dot{S}_2 &= \left(1 - \frac{S_2^*}{S_2}\right)\left((1-\rho)\pi - v\lambda S_2 - \mu S_2\right) \\ &= n_2\left(1 - \frac{S_2^*}{S_2}\right)\left(v\lambda^* S_2^* + \mu S_2^* - v\lambda S_2 - \mu S_2\right) \\ &= n_2 v\lambda^* S_2^*\left(1 - \frac{S_2^*}{S_2}\right)\left(1 - \frac{\lambda S_2}{\lambda^* S_2^*}\right) - \mu\frac{(S_2 - S_2^*)^2}{S_2} \\ &\leq n_2 v\lambda^* S_2^*\left(1 - \frac{\lambda S_2}{\lambda^* S_1^*} - \frac{S_2^*}{S_2} + \frac{\lambda}{\lambda^*}\right), \end{aligned} \tag{A-4}$$

and,

$$\begin{aligned} n_3\left(1 - \frac{E^*}{E}\right)\dot{E} &= \left(1 - \frac{E^*}{E}\right)\left(\lambda S_1 + v\lambda S_2 - g_1 E\right) \\ &= n_3\left(1 - \frac{E^*}{E}\right)\left(\lambda S_1 + v\lambda S_2 - (\lambda^* S_1^* + v\lambda^* S_2^*)\frac{E}{E^*}\right) \\ &= n_3\lambda^* S_1^*\left(1 - \frac{E^*}{E}\right)\left(\frac{\lambda S_1}{\lambda^* S_1^*} - \frac{E}{E^*}\right) + v\lambda^* S_2^*\left(1 - \frac{E^*}{E}\right)\left(\frac{\lambda S_2}{\lambda^* S_2^*} - \frac{E}{E^*}\right) \\ &= n_3\lambda^* S_1^*\left(\frac{\lambda S_1}{\lambda^* S_1^*} - \frac{E}{E^*} - \frac{\lambda S_1 E^*}{\lambda^* S_1^* E} + 1\right) + v\lambda^* S_2^*\left(\frac{\lambda S_2}{\lambda^* S_2^*} - \frac{E}{E^*} - \frac{\lambda S_2 E^*}{\lambda^* S_2^* E} + 1\right), \end{aligned} \tag{A-5}$$

and,

$$
\begin{aligned}
n_4\left(1-\frac{I^*}{I}\right)\dot{I} &= \left(1-\frac{I^*}{I}\right)\left(\sigma E - g_2 I\right) \\
&= n_4\left(1-\frac{I^*}{I}\right)\left(\sigma E - \sigma E^*\frac{I}{I^*}\right) \\
&= n_4\sigma E^*\left(1-\frac{I^*}{I}\right)\left(\frac{E}{E^*}-\frac{I}{I^*}\right) \\
&= n_4\sigma E^*\left(\frac{E}{E^*}-\frac{I}{I^*}-\frac{I^*E}{IE^*}+1\right),
\end{aligned}
\tag{A-6}
$$

and,

$$
\begin{aligned}
n_5\left(1-\frac{D^*}{D}\right)\dot{D} &= \left(1-\frac{D^*}{D}\right)\left(f\gamma I - \theta D\right) \\
&= n_5\left(1-\frac{D^*}{D}\right)\left(f\gamma I - f\gamma I^*\frac{D}{D^*}\right) \\
&= n_5 f\gamma I^*\left(1-\frac{D^*}{D}\right)\left(\frac{I}{I^*}-\frac{D}{D^*}\right) \\
&= n_5 f\gamma I^*\left(\frac{I}{I^*}-\frac{D}{D^*}-\frac{D^*I}{DI^*}+1\right).
\end{aligned}
\tag{A-7}
$$

Substituting $n_1 = n_2 = n_3 = 1$, $n_4 = \frac{\lambda^*}{\sigma E^*}(S_1^* + vS_2^*)$, and $n_5 = \frac{\lambda^* S_2^*}{f\gamma I^*}$, and equations (A-3)–(A-7) into equation (A-2), we have

$$
\begin{aligned}
\dot{V}(t) \leq & \lambda^* S_1^*\left(2-\frac{S_1^*}{S_1}-\frac{E}{E^*}-\frac{\lambda S_1 E^*}{\lambda^* S_1^* E}+\frac{\lambda}{\lambda^*}\right)+ \\
& v\lambda^* S_2^*\left(2-\frac{S_2^*}{S_2}-\frac{E}{E^*}-\frac{\lambda S_2 E^*}{\lambda^* S_2^* E}+\frac{\lambda}{\lambda^*}\right)+ \\
& \lambda^* S_1^*\left(\frac{E}{E^*}-\frac{I}{I^*}-\frac{I^*E}{IE^*}+1\right)+ \\
& v\lambda^* S_2^*\left(\frac{E}{E^*}-\frac{I}{I^*}-\frac{I^*E}{IE^*}+1\right)+ \\
& v\lambda^* S_2^*\left(\frac{I}{I^*}-\frac{D}{D^*}-\frac{D^*I}{DI^*}+1\right).
\end{aligned}
\tag{A-8}
$$

Suppose, a function is define as $u(x) = 1 - x + \ln x$, then, if $x > 0$ it leads to $u(x) \leq 0$. Also, if $x = 1$, then $u(x) = 0$. Implies that $x - 1 \geq \ln(x)$ for any $x > 0$ [20, 29, 30, 32, 33].
By using the above definition, direct calculation from equation (A-8), and conditions (i) and (ii), we have

$$
\begin{aligned}
&\left(2-\frac{S_1^*}{S_1}-\frac{E}{E^*}-\frac{\lambda S_1 E^*}{\lambda^* S_1^* E}+\frac{\lambda}{\lambda^*}\right) \\
&= \left(-(1-\frac{\lambda}{\lambda^*})(1-\frac{I\lambda^*}{I^*\lambda})+3-\frac{S_1^*}{S_1}-\frac{\lambda S_1 E^*}{\lambda^* S_1^* E}-\frac{I\lambda^*}{I^*\lambda}-\frac{E}{E^*}+\frac{I}{I^*}\right) \\
&\leq \left(-(\frac{S_1^*}{S_1}-1)-(\frac{\lambda S_1 E^*}{\lambda^* S_1^* E}-1)-(\frac{I\lambda^*}{I^*\lambda}-1)-\frac{E}{E^*}+\frac{I}{I^*}\right) \\
&\leq \left(-\ln(\frac{S_1^*}{S_1}\frac{\lambda S_1 E^*}{\lambda^* S_1^* E}\frac{I\lambda^*}{I^*\lambda})-\frac{E}{E^*}+\frac{I}{I^*}\right) \\
&= \left(\frac{I}{I^*}-\ln(\frac{I}{I^*})+\ln(\frac{E}{E^*})-\frac{E}{E^*}\right).
\end{aligned}
\tag{A-9}
$$

By using the above definition, direct calculation from equation (A-8), and conditions (i) and (ii) above, we have

$$\begin{aligned}
&\left(2-\frac{S_2^*}{S_2}-\frac{E}{E^*}-\frac{\lambda S_2 E^*}{\lambda^* S_2^* E}+\frac{\lambda}{\lambda^*}\right)\\
&=\left(-(1-\frac{\lambda}{\lambda^*})(1-\frac{D\lambda^*}{D^*\lambda})+3-\frac{S_2^*}{S_2}-\frac{\lambda S_2 E^*}{\lambda^* S_2^* E}-\frac{D\lambda^*}{D^*\lambda}-\frac{E}{E^*}+\frac{D}{D^*}\right)\\
&\leq\left(-(\frac{S_2^*}{S_2}-1)-(\frac{\lambda S_2 E^*}{\lambda^* S_2^* E}-1)-(\frac{D\lambda^*}{D^*\lambda}-1)-\frac{E}{E^*}+\frac{D}{D^*}\right)\\
&\leq\left(-\ln(\frac{S_2^*}{S_2}\frac{\lambda S_2 E^*}{\lambda^* S_2^* E}\frac{D\lambda^*}{D^*\lambda})-\frac{E}{E^*}+\frac{D}{D^*}\right)\\
&=\left(\frac{D}{D^*}-\ln(\frac{D}{D^*})+\ln(\frac{E}{E^*})-\frac{E}{E^*}\right).
\end{aligned} \tag{A-9}$$

Also from equation (A-8), we have

$$\frac{E}{E^*}-\frac{I}{I^*}-\frac{I^*E}{IE^*}+1=\left(u\left(\frac{I^*E}{IE^*}\right)+\frac{E}{E^*}-\ln\left(\frac{E}{E^*}\right)-\frac{I}{I^*}+\ln\left(\frac{I}{I^*}\right)\right)\leq\frac{E}{E^*}-\ln\left(\frac{E}{E^*}\right)+\ln\left(\frac{I}{I^*}\right)-\frac{I}{I^*}. \tag{A-10}$$

Similarly,

$$\frac{I}{I^*}-\frac{D}{D^*}-\frac{D^*I}{DI^*}+1=\left(u\left(\frac{D^*I}{DI^*}\right)+\frac{I}{I^*}-\ln\left(\frac{I}{I^*}\right)-\frac{D}{D^*}+\ln\left(\frac{D}{D^*}\right)\right)\leq\frac{I}{I^*}-\ln\left(\frac{I}{I^*}\right)+\ln\left(\frac{D}{D^*}\right)-\frac{D}{D^*}. \tag{A-11}$$

Hence,

$$\begin{aligned}
\dot{V}(t)=&\lambda^* S_1^*\left(\frac{I}{I^*}-\ln\left(\frac{I}{I^*}\right)+\ln\left(\frac{E}{E^*}\right)-\frac{E}{E^*}\right)+\\
&v\lambda^* S_2^*\left(\frac{D}{D^*}-\ln\left(\frac{D}{D^*}\right)+\ln\left(\frac{E}{E^*}\right)-\frac{E}{E^*}\right)+\\
&\lambda^* S_1^*\left(\frac{E}{E^*}-\ln\left(\frac{E}{E^*}\right)+\ln\left(\frac{I}{I^*}\right)-\frac{I}{I^*}\right)+\\
&v\lambda^* S_2^*\left(\frac{E}{E^*}-\ln\left(\frac{E}{E^*}\right)+\ln\left(\frac{I}{I^*}\right)-\frac{I}{I^*}\right)+\\
&v\lambda^* S_2^*\left(\frac{I}{I^*}-\ln\left(\frac{I}{I^*}\right)+\ln\left(\frac{D}{D^*}\right)-\frac{D}{D^*}\right).
\end{aligned} \tag{A-13}$$

Equations (A-3)–(A-13) ensure that $\dot{V(t)}\leq 0$. Further, the equality $\frac{dV}{dt}=0$ holds only if $S_1=S_1^*$, $S_2=S_2^*$ $E=E^*$, $I=I^*$, and $D=D^*$. Thus, the endemic equilibrium state (3.3), is the only positive invariant set to the system (2.1) contained entirely in $\left\{(S_1,S_2,E,I,D)\in\Omega: S_1=S_1^*,S_2=S_2^*,E=E^*,I=I^*,D=D^*\right\}$. Hence, it follows from the LaSalle's invariance principle [44] that every solutions to the equations (2.1) with initial conditions in Ω converge to endemic equilibrium point, Γ^*, as $t\to\infty$. Thus, the positive endemic equilibrium is globally asymptotically stable.